Progress In Electromagnetics Research C, Vol. 123, 27–43, 2022

Third Order U-Shaped Quasi-Reflectionless Bandpass Filter

Bahaa H. Alkhuwaildi* **and Nasr Alkhafaji**

Abstract—A filter with good impedance matching for both in-band and a wide range of out-of-band is reported in this paper. Thus, the proposed filter offers low reflection for a wide range of frequencies, and it can be called as quasi-reflectionless filter. Also, the proposed filter improves the passband flatness significantly. The quasi-reflectionless filter consists of n-pole conventional U-shaped bandpass filters with absorptive stubs (ABSs) placed at the input and output ports. Each part in the whole filter is individually investigated. The U-shaped resonator is studied first, and then the ABSs are analyzed mathematically and simulated to optimize the attenuation rejection. Several parameters that have an influence on the overall performance are investigated. Different n-pole filters are simulated to simply enhance the out-of-band rejection without affecting the passband response. The filter response is furthermore improved by introducing two transmission zeros using the cross-coupling between the two ABSs. To validate the proposed idea, the 3-pole U-shaped quasi-reflectionless BPF is fabricated on an FR4 substrate at the operating frequency of 3.5 GHz. The filter has measured responses very close to the simulated ones.

1. INTRODUCTION

Nowadays, wireless communication systems become an essential part in our life. To get good performance, the fundamental parts in the radio-frequency RF chains should be always developed. Microwave filter is one of those parts. Filters operate to pass a certain range of frequencies (i.e., the channel bandwidth), while other frequencies will be rejected. In conventional filters, the rejected signals will be reflected back from where they come due to high mismatching. This reflection will cause deterioration in the performance of nonlinear devices such as mixers, amplifiers, and oscillators. To circumvent this problem, the solution is to use to use nonreciprocal circulator or isolator to redirect the reflected power into absorptive loads. However, this solution will complicate the design and increase the cost [1]. To avoid using bulky conventional nonreciprocal devices, reflectionless filters have attracted a lot of attention recently. These filters have the ability to mitigate the reflected signals for all frequencies for passbands and stopbands, so they are called reflectionless filters. There are also quasi-reflectionless filters, being able to decrease the reflected signals for a wide range of stopband frequencies. The reflected signals are dissipated inside the filter itself by the absorptive parts. Thus, the filter is well matched not only for the passband but also for the stopband [2].

To do so, designers have reported several schemes such as complementary duplexer, lossy resonators, and directional filter. The filters can be designed using either lumped elements or transmission lines. When using lumped elements, even-odd mode analysis will be an appropriate way to design reflectionless filters. In [3], a new class of reflectionless filter was designed. The circuits are symmetrical, so the even and odd modes of the S_{11} have the same magnitudes but with opposite phases, resulting in the cancellation of S_{11}. The authors also introduced the procedure to convert from lowpass filters

Received 12 June 2022, Accepted 3 August 2022, Scheduled 19 August 2022

* Corresponding author: Bahaa Hamzah Alkhuwaildi (bahaa.jasim.ms.etcn@student.atu.edu.iq).
The authors are with the Department of Communication Engineering Techniques, Engineering Technical College of Al-Najaf, Al-Furat Al-Awsat Technical University, Najaf, Iraq.

into highpass filters, bandpass filters, and bandstop filters with all mathematical background. In [4], an extended work of the previous concepts in [3] is introduced. N-order distributed counterpart reflectionless filters relied on lowpass prototypes are reported in [5]. The main channel contains only one resonator, while the absorptive part can be any order to enhance the filter response. To obtain a certain transmission response, symmetrical lumped reflectionless filter is proposed [6]. The design requires a large number of lumped elements with operation frequency limitations associated with the lumped elements, so this problem is solved in [7] using the distributed (transmission lines). Richards and Kuroda identities transformations are utilized.

One of the other important schemes of reflectionless filters is complementary duplexer which consists of two channels; the main one is to pass the interesting signals from the input to the output, while the other is to absorb the unwanted signals [8, 9]. In [10], the authors used only one absorptive stub located at the input port to reduce the reflections exploiting the complementary duplexer technique. The same previous idea is also used in [11], but the filter is multiband where even the absorptive stub is multiband stop filter. However, in [12], a symmetric quasi-reflectionless filter is reported by adding the absorptive stubs at both two ports. The two absorptive stubs are the same order.

Reflectionless filters, based on lossy stubs, consist of a transmission line (stub) in series with an absorptive resistor to mitigate the reflection. Absorptive bandstop filters based on lossy resonator are presented in [13–18]. In [19], only one port 3-pole distributed absorptive bandpass filter in which the first resonator is loaded with a resistor in series with a short stub, while in [20, 21], absorptive stubs are placed on the two ports of coupled lined BPF to realize symmetrical quasi-reflectionless response for a wide band of frequencies. Another topology to implement reflectionless BPFs is the use of directional filters [22–24], but this type has disadvantages such as high insertion loss, limited bandwidth, and large size. In this paper, the reflection coefficient S_{11} is very low using one-order absorptive stubs compared to other works using higher orders of absorptive stubs to obtain almost identical responses. Also, the bandpass filter (BPF) (the main channel) is a U-shaped microstrip bandpass filter which is used for the first time in the design of quasi-reflectionless filters according to the best of authors' knowledge.

The paper is organized as follows. Section 2 introduces the required mathematical background and investigations for the proposed design. This section is divided into three parts, and each part discusses a specific topic. In Section 3, a U-shaped quasi-reflectionless bandpass filter design is presented. Several parameters will be investigated to optimize the overall performance. Next, the design procedure is provided. The experimental validation compares between the simulated and measured results in Section 4. Also, this section provides the comparison between this work and others in the literature. Finally, the conclusion is drawn.

2. MATHEMATICAL BACKGROUND OF THE PROPOSED FILTER

In this section, the main points discussing the mathematical background and main filter parts are introduced. First, a conventional U-shaped BPF is discussed (first part). The second part explains the operation of absorptive stubs (ABSs). The last part determines the input impedance of one-port U-shaped quasi-reflectionless BPF design.

2.1. U-Shaped Bandpass Filter

The conventional U-shaped coupled resonators are first examined since they consider the core of our proposed work. The straight $\lambda/2$ resonators are large compared to the U-shaped resonators, so the latter type is adopted in our structure. Moreover, the input and output ports can be placed close to each other to enhance the filter selectivity by adding zeros into the filter response. The U-shaped figure comes from folding the arms of the straight $\lambda/2$ resonators into U shape to reduce the size as shown in Fig. 1. Several U-shaped resonators are adjacently placed, and the amount of power transferred among them relies on the space separating them, like the parallel coupled resonators. Hence, the same design equations for parallel coupled $\lambda/2$ resonators can be used. However, to fold the resonators, it is necessary to take into account the reduction in the coupling length, which in turn, reduces the coupling between the resonators. The coupled length is slightly less than a quarter wavelength because each resonator has two bends, and there should be a distance to separate them [25]. To design the U-shaped

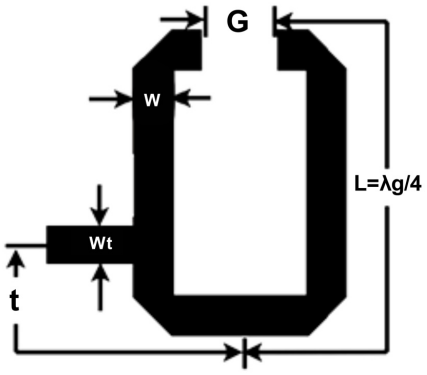

Figure 1. The U-shaped bandpass resonator.

bandpass filter, the classical filter methodology can be utilized [26]

$$Q_{e1} = \frac{g_0 g_1}{FBW}, \quad Q_{en} = \frac{g_n g_{n+1}}{FBW} \tag{1}$$

$$M_{i,i+1} = \frac{FBW}{\sqrt{g_i g_{i+1}}} \tag{2}$$

where Q_{e1} and Q_{en} are the external quality factors of the resonators at the input and output, respectively, and $M_{i,i+1}$ are the coupling coefficients between the two adjacent resonators. g_i is the i-th normalized filter element. FBW is the fractional bandwidth. The feeding method used is a tapped-line which is a $50\,\Omega$ microstrip input (output) feeding transmission line. The location of tapped-line feed is approximately given by:

$$t = \frac{2L}{\pi} \sin^{-1}\left(\sqrt{\frac{\pi Z_0}{2Q_\theta Z_f}}\right) \tag{3}$$

where Z_f is the characteristic impedance of the transmission line forming the U-shaped resonator, Z_0 the characteristic impedance of feeding input (output) transmission line, and L half the length of the

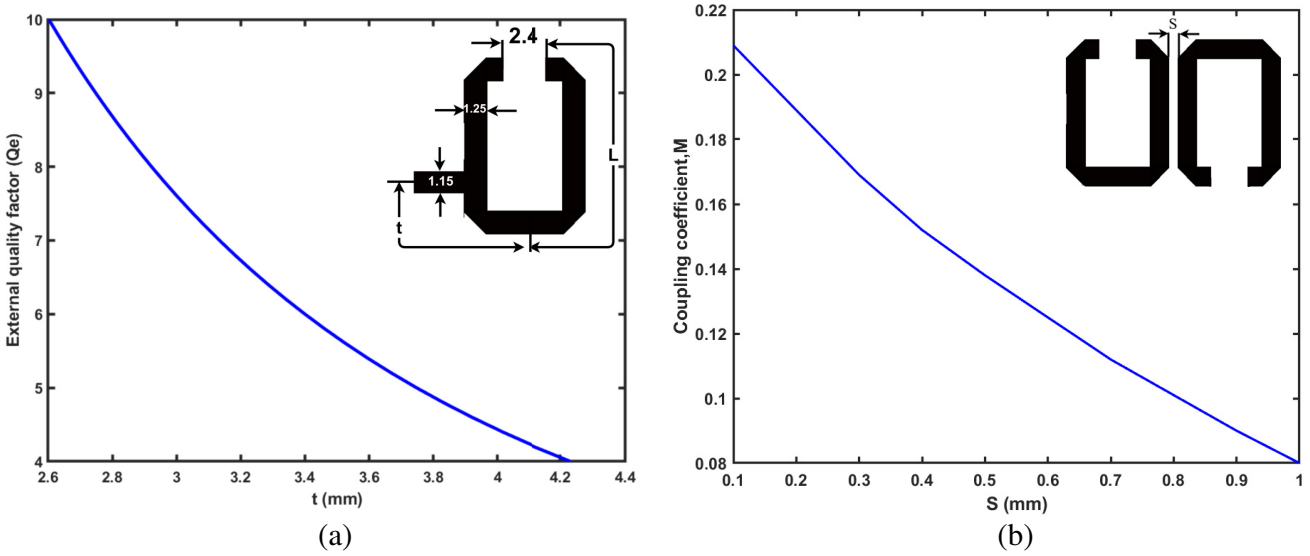

(a) (b)

Figure 2. Design curves obtained by ADS simulations for designing the microstrip U-shaped BPF, (a) external quality factor, (b) coupling coefficient.

single resonator which is about a quarter wavelength at the design frequency. The advanced system design (ADS) is used to extract the external quality factor and coupling coefficients. Fig. 2 shows these two parameters. As can be seen in Fig. 2(a), the feeding location (t) plays a vital role in how to control the external quality factor. The external quality factor decreases as t increases. Less input power can be injected into the resonator when t increases. In other words, when the feeding transmission line approaches the open-end of the resonator, the power coupling between the feeding transmission line and resonator decreases. Moreover, the space between the adjacent resonators controls the amount of power transferred between them, see Fig. 2(b). Thus, these two parameters (i.e., Q_e, and M) are investigated and optimized carefully.

2.2. Absorptive Stub (ABS)

In this part, a detailed analysis of converting one pole bandstop filter to absorptive stub (ABS) is provided. Instead of using the output port, it is replaced by a resistor as shown in Fig. 3. The resistor absorbs the power. Fig. 3 illustrates the conversion procedure of the ABS. In Fig. 3(a), an open-end quarter wavelength shunt stub is proposed as first order bandstop filter. Z_{st} and θ_{st} are its characteristic impedance and its electrical length. Z_A and Z_B denote the input and output port impedances, respectively. The electrical length of $\theta_{st} = 90$ at the stopband center frequency f_0. The impedance parameters of the bandstop filter circuit can be extracted from its lowpass filter prototype as follows [26]:

$$\begin{aligned} Z_A &= g_0 Z_0, \quad Z_B = \frac{Z_A g_2}{g_0} \\ Z_{st} &= \frac{Z_A}{\alpha g_0 g_1} \\ \alpha &= \cot\left(\frac{\pi}{2}\left(1 - \frac{FBW}{2}\right)\right) \\ FBW &= \frac{f_2 - f_1}{f_0}, \quad f_0 = \sqrt{f_1 f_2} \end{aligned} \tag{4}$$

where α is the bandwidth parameter, and f_1 and f_2 are frequency points in the bandstop response.

$$Z_{in1} = -jZ_{st}\cot(\theta_{st}) \tag{5}$$

where Z_{in1} is the input impedance of shunt stub. If Z_{st} increases, it may lead to obtain narrower FBW. This causes a serious difficulty in implementation. To circumvent this problem, another transmission line with an electrical length of $\theta_3 = 180°$ and a characteristic impedance of Z_3 is added in series into the shunt stub as shown in Fig. 3(b). The input impedance seen at the beginning of the shunt stub can be calculated as in

$$Z_{in2} = Z_2 \frac{-jZ_3\cot(\theta_3) + jZ_2\tan(\theta_2)}{Z_2 + Z_3\cot(\theta_3)\tan(\theta_2)} \tag{6}$$

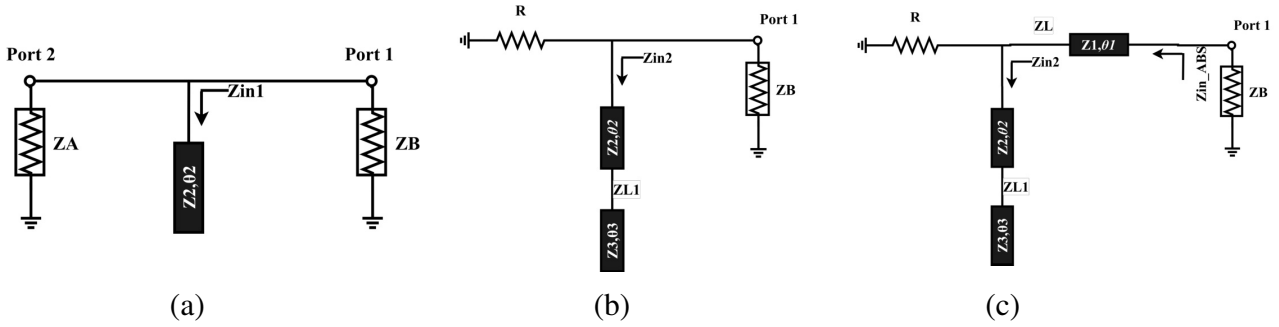

Figure 3. The procedure of converting the conventional one-pole band stop filter into its ABS counterpart, (a) the conventional one-pole bandstop filter (transmission line model), (b) the conventional one-pole bandstop filter (simplified circuit with the same responses), (c) the proposed absorptive filter.

Z_{in2} can be matched to the input port by inserting a quarter-wavelength transformer, with an impedance of Z_1 and electrical length of θ_1, between the input port and the shunt stub. Then, the input impedance of entire absorptive part Z_{in-ABS}, depicted in Fig. 3(c), is:

$$\begin{aligned} Z_{in-ABS} &= Z_1 \frac{Z_L + jZ_1 \tan(\theta_1)}{Z_1 + jZ_L \tan(\theta_1)} \\ Z_L &= \frac{-jRZ_2Z_3 \cot(\theta_3) + jRZ_2^2 \tan(\theta_2)}{-jZ_2Z_3 \cot(\theta_3) + jZ_2^2 \tan(\theta_2) + jRZ_3 \cot(\theta_3) + jRZ_2 \tan(\theta_2)} \end{aligned} \tag{7}$$

For any lossless two-port network, such as the one in Fig. 3(a), the conservation of power requires [1]:

$$|S_{11}|^2 + |S_{21}|^2 = 1 \tag{8}$$

while for the absorptive single-port circuit depicted in Fig. 3(c), the power is either reflected back to port 1 or absorbed by the resistor R. Here, we define S_{11-ABS} and S_{a-ABS} as the reflection and absorption coefficients of the absorptive filter, respectively. Therefore, we have:

$$|S_{11-ABS}|^2 + |S_{a-ABS}|^2 = 1 \tag{9}$$

Figure 4 compares the responses resulting from the designs depicted in Fig. 3. The reflection coefficient (S_{11}), transmission or absorption coefficients (S_{21}), and the magnitudes of input impedances are provided. Here, a bandstop filter operating at 3.5 GHz with 0.1 dB passband ripple and 83% stopband fractional bandwidth is used as an example. The circuits in Fig. 3 were analyzed, designed, and simulated at 3.5 GHz, where the x-axes show the normalized frequencies. The lowpass prototype element values are found to be $g_0 = 1$, $g_1 = 0.3052$, $g_2 = 1$. The circuit parameters of BSF are $Z_A = 50\,\Omega$, $Z_B = 50\,\Omega$, $Z_{st} = 211.5\,\Omega$, and the parameters of ABS are $R = 50\,\Omega$, $Z_1 = 56.5\,\Omega$, $Z_2 = 71.5\,\Omega$, $Z_3 = 71.5\,\Omega$, $\theta_1 = \theta_2 = 90°$, and $\theta_3 = 180°$.

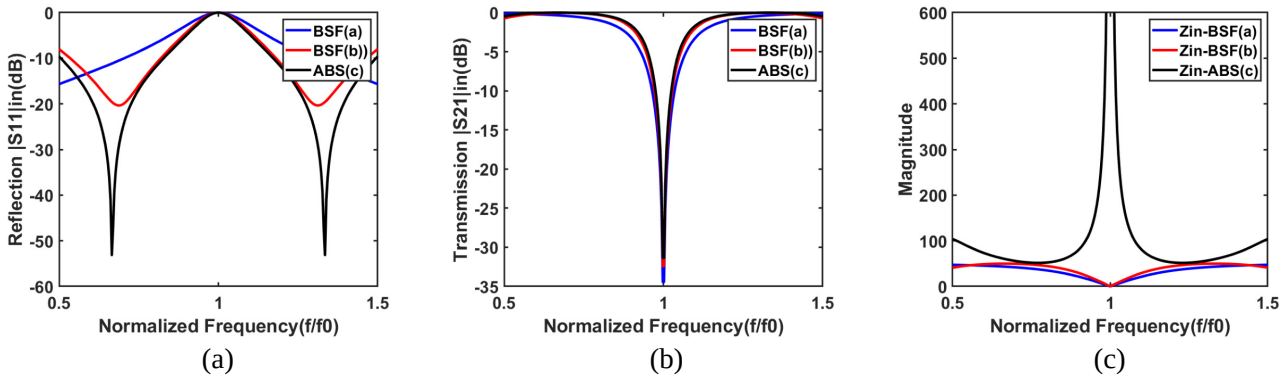

Figure 4. Reflection and transmission (absorption) coefficients, and magnitudes of the input impedances for the designs evolved in Fig. 3. (a) Reflection S_{11}, (b) transmission S_{21}, (c) magnitudes of the input impedances $mag(Z)$.

The blue lines represent responses of the BSF(a), and the responses confirm the BSF behavior. Although the BSF(b) has one port, its responses (red lines) are the same as the former one. Away from the resonance, the power will be absorbed by the resistor (Fig. 3(b)) instead of being transferred into the output port (Fig. 3(a)). At the resonance, both the first two designs have short circuit input impedances. Thus, the reflected signals will be out-of-phase with the main RF signals, and the destructive interference will occur. In our proposed design, the input impedance should be very high (i.e., close to the open circuit behavior) to ensure that the RF signals can pass directly to the main bandpass filter. The last design in Fig. 3 uses an impedance inverter which is a quarter-wavelength transmission line. As demonstrated in Fig. 3(c), the input impedance is very high, more than 500 Ω, guaranteed to make the instructive interference. Also, there are two symmetrical transmission poles located before and after the resonance frequency. They aid to enhance the overall performance.

There are a few observations obtained from Figs. 3 and 4:

1. Circuit in Fig. 3(b) is an equivalent to circuit Fig. 3(a) in terms of a magnitude of the input impedance.
2. Fig. 4(c) shows the $mag(Z_{in-BSF})$ and $mag(Z_{in-ABS})$. The value of $mag(Z_{in-BSF})$ at the resonant frequency is zero (i.e., short circuit), whereas the value of $mag(Z_{in-ABS})$ is optimized to be as high as possible.
3. Fig. 4(b) demonstrates that all the three circuits introduced in Fig. 3 have the same transmission (absorption) in both the stopband and passband.

2.3. Input Impedance of One-Port U-Shaped Quasi-Reflectionless BPF

The U-shaped quasi-reflectionless bandpass filter based on the complimentary duplexer method will be designed and analyzed here. It has two channels. The first (main) channel is to pass the desired signals into the output (i.e., the BPF), while the second (auxiliary) channel is to absorb the undesired signals (i.e., the ABS). Fig. 5 shows the proposed filter but with only the input port and one ABS for the sake of simplicity. Z_{in} is the input impedance at port one which represents the parallel combination of the input impedance of the U-shaped $BPF(Z_{in-BPF})$ and the input impedance of the absorptive stub (Z_{in-ABS}). Z_{in} can be written as:

$$Z_{in} = \frac{Z_{in-BPF} * Z_{in-ABS}}{Z_{in-BPF} + Z_{in-ABS}} \tag{10}$$

The reflection coefficient (S_{11}) of the quasi-reflectionless bandpass filter is:

$$S_{11} = \frac{Z_{in} - Z_0}{Z_{in} + Z_0} \tag{11}$$

To further explore the mechanism of reflectionless behavior, the magnitude of Z_{in} must be matched to Z_0 at all frequencies. However, the magnitude of Z_{in-BPF} should be matched to Z_0 at in-band frequencies and mismatched at out-of-band frequencies, whereas the magnitude of Z_{in-ABS} should be mismatched to Z_0 at in-band frequencies and matched to Z_0 at out-of-band frequencies. This theoretical explanation results in S_{11} equal to zero at all frequencies. Practically, this is impossible because the input impedances of the two channels forming the quasi-reflectionless BPF are functions with frequency and not equal to $50\,\Omega$ throughout a frequency range. However, the proposed design offers the input impedance close to $50\,\Omega$ at a wide frequency range. Fig. 6 displays the magnitudes of Z_{in-BPF} and Z_{in-ABS}. It is evident from the results that when the BPF is matched, the ABS is mismatched, and vice versa.

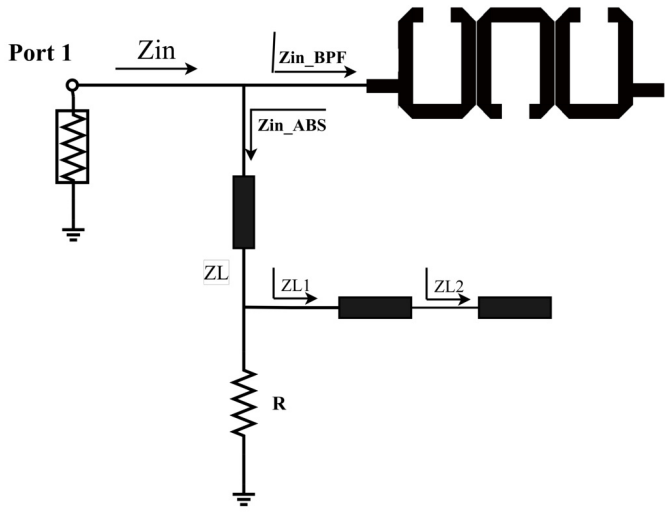

Figure 5. U-shaped quasi-reflectionless BPF.

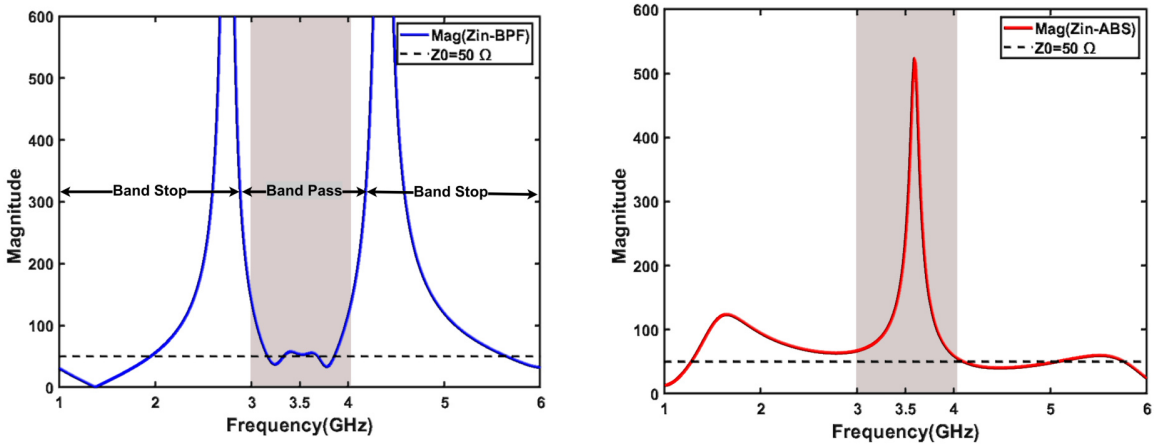

Figure 6. Input impedance of one-port U-shaped quasi-reflectionless, (a) magnitude (Z_{in-BPF}), (b) magnitude (Z_{in-ABS}).

3. U-SHAPED QUASI-REFLECTIONLESS BANDPASS FILTER DESIGN

This section is divided into four parts. The first part deals with the design of conventional and quasi-reflectionless 3-pole U-shaped BPF. Then, in the second part, discussing effects of the ABS stub on the overall bandwidth of the proposed design is introduced. Next, U-shaped quasi-reflectionless filters with various orders are investigated. Ultimately, improving the out-of-band rejection based on the cross-coupling technique is presented.

3.1. 3-Pole U-Shaped Quasi-Reflectionless BPF

In this subsection, the 3-pole U-shaped quasi-reflectionless BPF is designed and analyzed. For this design, the fractional bandwidth $FBW = 20\%$ or $FBW = 0.2$ at a resonant frequency $f_0 = 3.5\,\text{GHz}$, $n = 3$ (Butterworth lowpass type). The lowpass prototype parameters, with respect to a normalized lowpass cutoff frequency $\omega_c = 1$, are $g_0 = 1$, $g_1 = 1$, $g_2 = 2$, and $g_3 = 1$. Table 1 shows the physical dimensions of 3-pole U-shaped BPF relying on Eqs. (1)–(3), and curves are provided in Fig. 2. In Fig. 7(b), two ABSs are connected into the output and input ports, converting the conventional bandpass filter into the quasi-reflectionless bandpass filter. The parameters $(a1, a2, a3)$, shown in Fig. 7(b), are scaling factors used to optimize the performance of the transmission and absorption. Figs. 8–11 show the parametric studies of the reflection and transmission coefficients and the magnitude of input impedance of the U-shaped quasi-reflectionless bandpass filter. The nominal values of the various parameters are the same as those in the example given in Section 2.2. As can be observed, the bandwidth of the

Table 1. The physical dimensions of U-shaped BPF.

parameters	Measurements in (mm)
Length (L)	10.05
Taped input Length (L_t)	2.62
Space between the resonators (S)	0.5
Gap between open end of U-shaped BPF (G)	2.4
Width (W)	1.25
Width of feed (W_t)	1.15
Taped input (t)	3.75

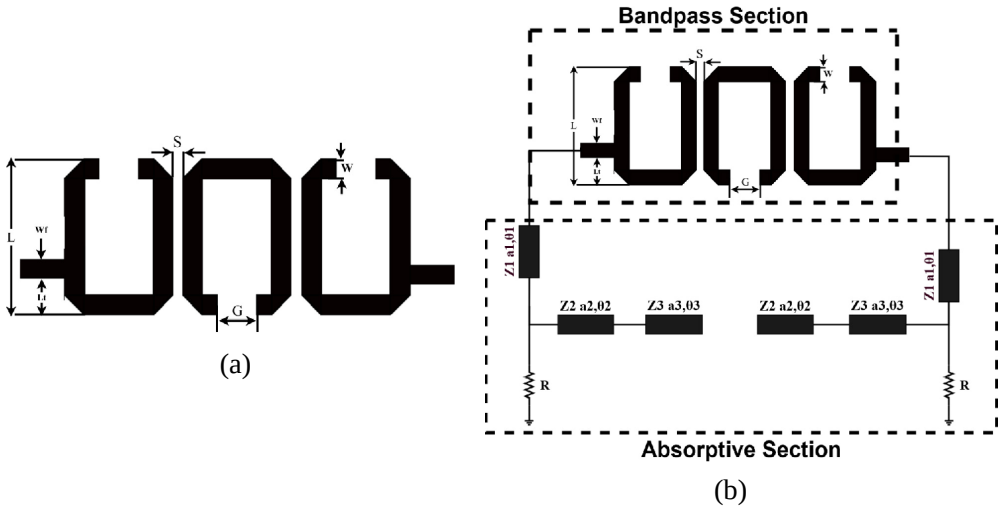

Figure 7. (a) The layout of 3-pole U-shaped BPF, (b) the layout of 3-pole U-shaped BPF with the transmission line circuit model of the ABSs connected into the output and input ports.

quasi-reflectionless filter is mainly determined by the bandwidth of the absorptive filter that will be discussed in the subsequent part. Typically, the U-shaped BPF provides larger bandwidth than the ABSs [5], where spacing (S) between the U-shaped resonators governs the bandwidth of the BPF. Thus, the goal is to make the ABS have a bandwidth as wide as possible. Fig. 8 exhibits the frequency responses of the proposed filter shown in Fig. 7(b) for different values of s. The widest bandwidth can be obtained if $S = 0.2\,\text{mm}$, because the bandwidth of the U-shaped bandpass filter becomes larger than the reflection bandwidth of the ABS, so we can leverage from this point to obtain the possible widest bandwidth. However, for practical issues such as the fabrication tolerances using the chemical etching method, $S = 0.5\,\text{mm}$ was chosen.

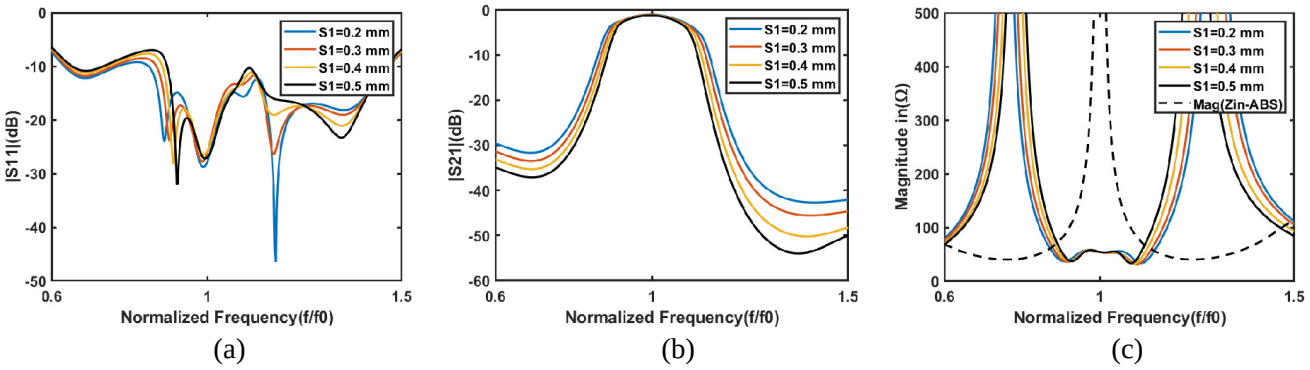

Figure 8. Simulated frequency responses of the 3-pole U-shaped quasi-reflectionless BPF with respect to S ($Z_0 = 50\,\Omega$, $Z_1 = Z_0 * a1\,\Omega, Z_2 = Z_0 * a2\,\Omega, Z_3 = Z_0 * a3\,\Omega, \theta_1 = \theta_2 = 90°, \theta_3 = 180°, a1 = 1, a2 = 1, a3 = 1$).

Moreover, the values of $a1, a2$ and $a3$ can be adjusted to improve the absorption performance (i.e., reducing the reflection in out-of the passband and even inside the passband). In other words, the reflected signals from the main channel of the proposed filter will be largely directed into the absorption branch, the ABS. As shown in Fig. 9, the value of $a1 = 1.128$. When $a1 = 0.9$, the wide band of absorption is noticed, but the filter offers higher reflection than the response when $a1 = 1.128$. Also, the filter transmission deteriorates. Here, $a2$ is varied to investigate its influences on the overall performance of the proposed filter. Fig. 10 demonstrates the best value of $a2 = 1.43$ in terms of the

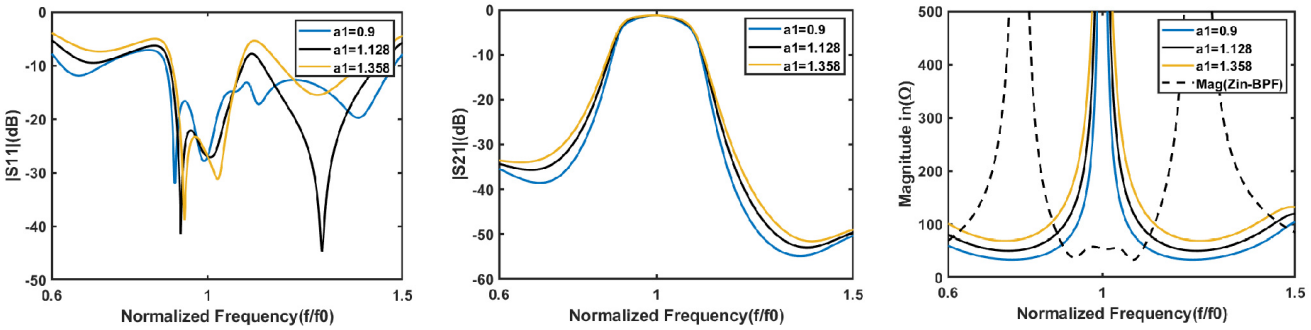

Figure 9. Simulated frequency responses of the 3-pole U-shaped quasi-reflectionless BPF with respect to $a1$ ($Z_0 = 50\,\Omega$, $Z_1 = Z_0 * a1\,\Omega, Z_2 = Z_0 * a2\,\Omega, Z_3 = Z_0 * a3\,\Omega, \theta_1 = \theta_2 = 90°, \theta_3 = 180°, a2 = 1, a3 = 1, S = 0.5\,\text{mm}$).

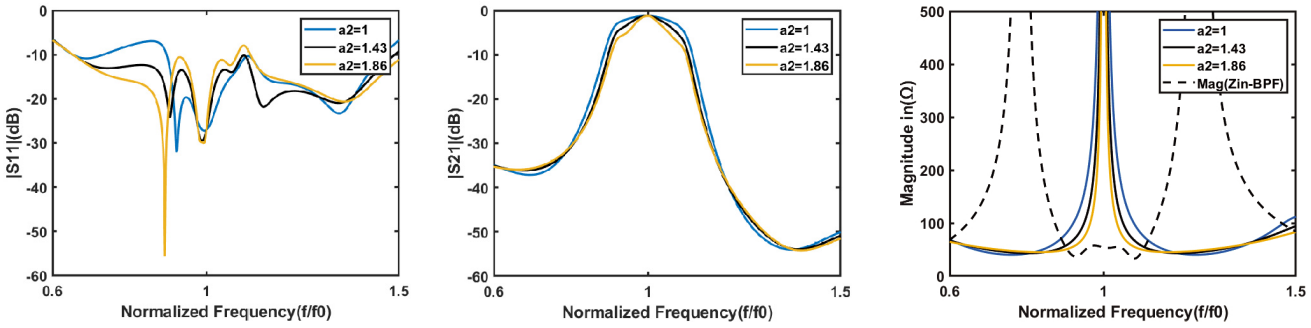

Figure 10. Simulated frequency responses of the 3-pole U-shaped quasi-reflectionless BPF with respect to $a2$ ($Z_0 = 50\,\Omega$, $Z_1 = Z_0 * a1\,\Omega, Z_2 = Z_0 * a2\,\Omega, Z_3 = Z_0 * a3\,\Omega, \theta_1 = \theta_2 = 90°, \theta_3 = 180°, a1 = 1.128, a3 = 1, S = 0.5\,\text{mm}$).

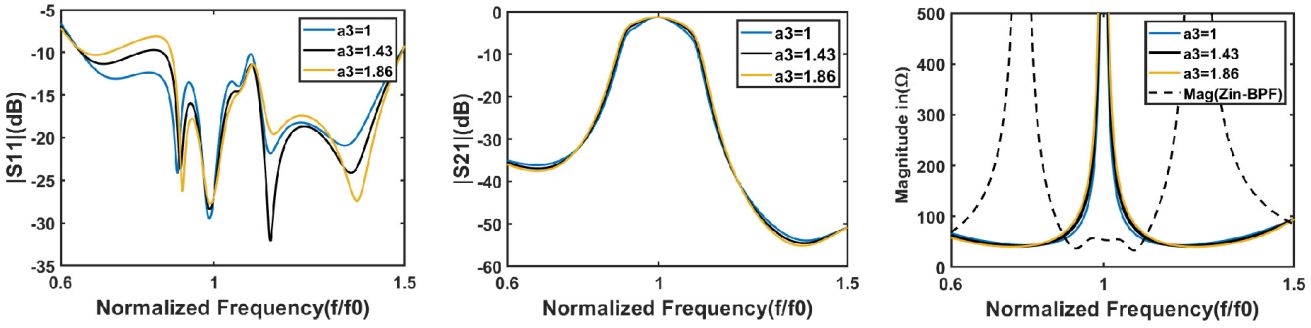

Figure 11. Simulated frequency responses of the 3-pole U-shaped quasi-reflectionless BPF with respect to $a3$ ($Z_0 = 50\,\Omega$, $Z_1 = Z_0 * a1\,\Omega, Z_2 = Z_0 * a2\,\Omega, Z_3 = Z_0 * a3\,\Omega, \theta_1 = \theta_2 = 90°, \theta_3 = 180°, a1 = 1.128, a2 = 1.43, S = 0.5\,\text{mm}$).

absorption. The matching between Z_{in-BPF} and Z_{in-ABS} is increased because the value of reflection is decreased for the out-of-band of the normalized frequency (f/f_0) ranging from 0.65 to 0.9 (less than 12 dB), and from 1.12 to 1.145 (less than 15 dB). In addition, the increase in the matching inside the band is achieved, although we find that the value of the transmission deteriorates slightly. The value of $a3$ is also chosen to be 1.43, see Fig. 11.

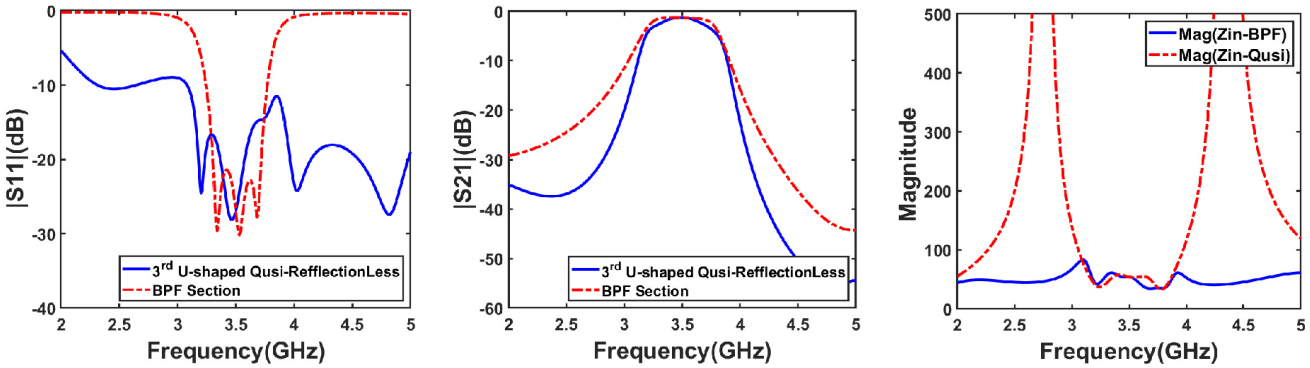

Figure 12. Simulated frequency responses of the 3-pole U-shaped quasi-reflectionless BPF and its bandpass section ($Z_1 = 56.4\,\Omega$, $Z_2 = 71.5\,\Omega, Z_3 = 71.5\,\Omega, \theta_1 = \theta_2 = 90°, \theta_3 = 180°, a1 = 1.128, a2 = 1.43, a3 = 1.43, S = 0.5\,\text{mm}$).

To this end, the most important parameters of the proposed design were optimized. Fig. 12 shows the transmission and reflection coefficients and the magnitude of input impedance for the optimized 3-pole U-shaped quasi-reflectionless bandpass filter and the conventional 3-pole U-shaped BPF. Obviously, both designs given in Fig. 7 show the same transmission characteristics with a passband centered at 3.5 GHz and two cutoff frequencies ($f1 = 3.16\,\text{GHz}$) and ($f2 = 3.83\,\text{GHz}$). The filter in Fig. 7(b) has higher selectivity and sharper roll-off than the design in Fig. 7(a), thanks to the ABS section. The reduction in the reflection coefficient is very apparent. In other words, the quasi-reflection less property is satisfied. The dashed red line in Fig. 12 shows three reflection zeros in the reflection coefficient response to confirm that the filter consists of three resonators. More reflection zeros are added by the ABS to the full response of the proposed design (i.e., the blue solid line). The proposed design has input impedance almost equal to $50\,\Omega$ of 2 GHz to 5.5 GHz, although there is a ripple in the center frequency owing to the change in the phase of the transmitted signal near the resonance. The input impedance is between $32.3\,\Omega$ and $83\,\Omega$ at the that frequency range. The reflection response of the 3-pole U-shaped quasi-reflectionless filter is below $-20\,\text{dB}$ across the frequency range of 3.96 GHz–4.07 GHz and near $-10\,\text{dB}$ for the range of 2.18 GHz–3.012 GHz. Also, full matching inside the passband is carried out, and the ABS filter helps to eliminate out-of-band signals near the passband and significantly improves the close-in rejection.

3.2. Discussion on the Filter Bandwidth

Figure 13 compares the transmission coefficient of the 3-pole quasi-reflectionless filter $|S_{21-Q}|$, the reflection coefficient of its absorptive filter $|S_{11-ABS}|$, and the transmission coefficient of BPF section. Here, the subscript Q and ABS stand for quasi-reflectionless BPF and absorptive filter, respectively. From Fig. 13, we can see that S_{21-Q} (blue line) is almost the same as $|S_{11-ABS}|$ in terms of the bandwidth. A qualitative explanation can be offered as follows. In a resistor-embedded circuit (i.e., the quasi-reflectionless filter) of Fig. 7, the input signal power is either reflected, transmitted, or absorbed. The conservation of power requires

$$|S_{11-Q}|^2 + |S_{21-Q}|^2 + |S_{a-Q}|^2 = 1 \tag{12}$$

where S_{a-Q} is the absorption coefficient of the quasi-reflectionless BPF. Since $S_{11-Q} \approx 0$ for the quasi-reflectionless filter within the operating bandwidth, (12) is reduced to

$$|S_{21-Q}|^2 + |S_{a-Q}|^2 = 1 \tag{13}$$

Comparing (9) and (13) leads to the conclusion that $S_{21-Q} = S_{11-ABS}$ [21]. From this math, the transmission coefficient of the quasi-reflectionless bandpass filter is close to the reflection coefficient of the ABS branch under some restrictions such as slight difference in the impedances. Therefore, the

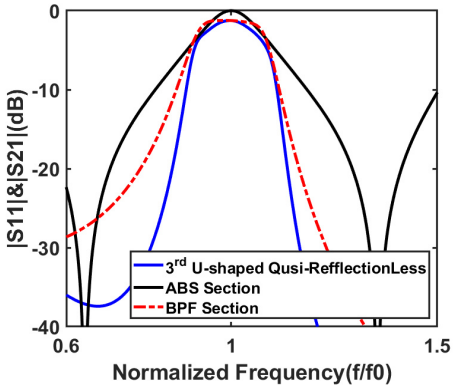

Figure 13. Simulated comparison between the transmission of U-shaped quasi-reflectionless BPF (Fig. 7) and the reflection of absorptive filter in (Fig. 3(c)).

quasi-reflectionless BPF has almost identical BW3 dB (passband) to the BW3 dB (reflection) for the ABS.

To remark the main points, this procedure can be considered as an initial step to design and synthesize the reflectionless filters in terms of the bandwidth requirements.

3.3. Extension to Higher-Order Designs

Adding more resonators to the BPF branch enhances the filter selectivity but at the cost of design complexity and size. Thus, a filter satisfying the prescribed design requirements with lower number of resonators is the aim of most filter designers. As in Fig. 7, extending the filter order is achieved. Higher-order quasi-reflectionless BPFs can be readily realized by cascading more U-shaped resonators. Figs. 14(a) and 14(b) show examples of the 4- and 5-pole U-shaped quasi-reflectionless filters, respectively. Note that the added U-shaped resonators have the same parameters as that for the resonators in the 3-pole proposed filter.

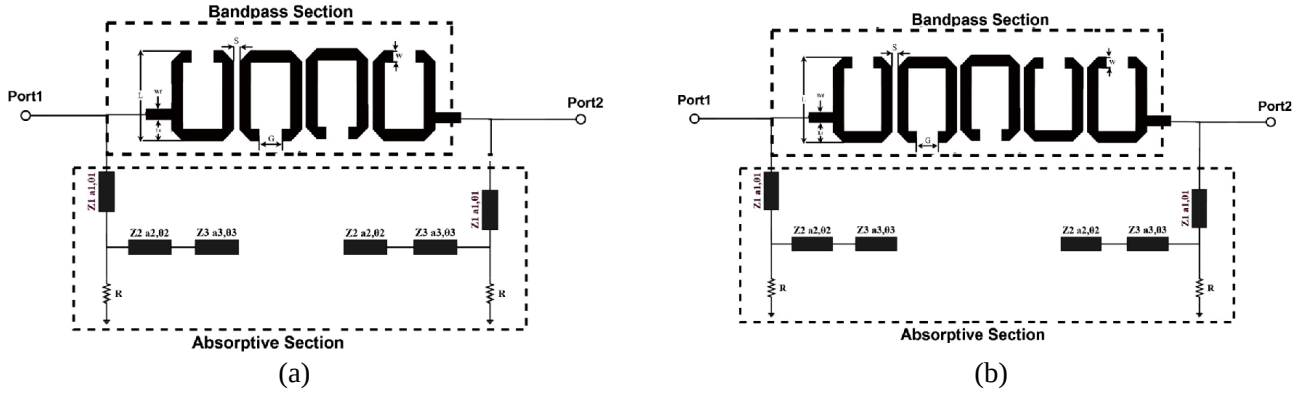

Figure 14. The layout of n-pole U-shaped BPF with the transmission line circuit model of the ABSs connected into the output and input ports, (a) 4th order, (b) 5th order.

Figures 15(a) and (b) show the frequency responses (reflection, transmission, and input impedance) of the 4-pole and 5-pole U-shaped quasi-reflectionless filters with varying S, respectively. $a1$, $a2$, and $a3$ are assumed the same as in the optimized 3-pole quasi-reflectionless BPF. As S changes, the frequency responses of the higher order filters do not change noticeably. The reason is that the rejection bandwidth of the ABS is larger than the bandwidth of the main channel of the proposed filter.

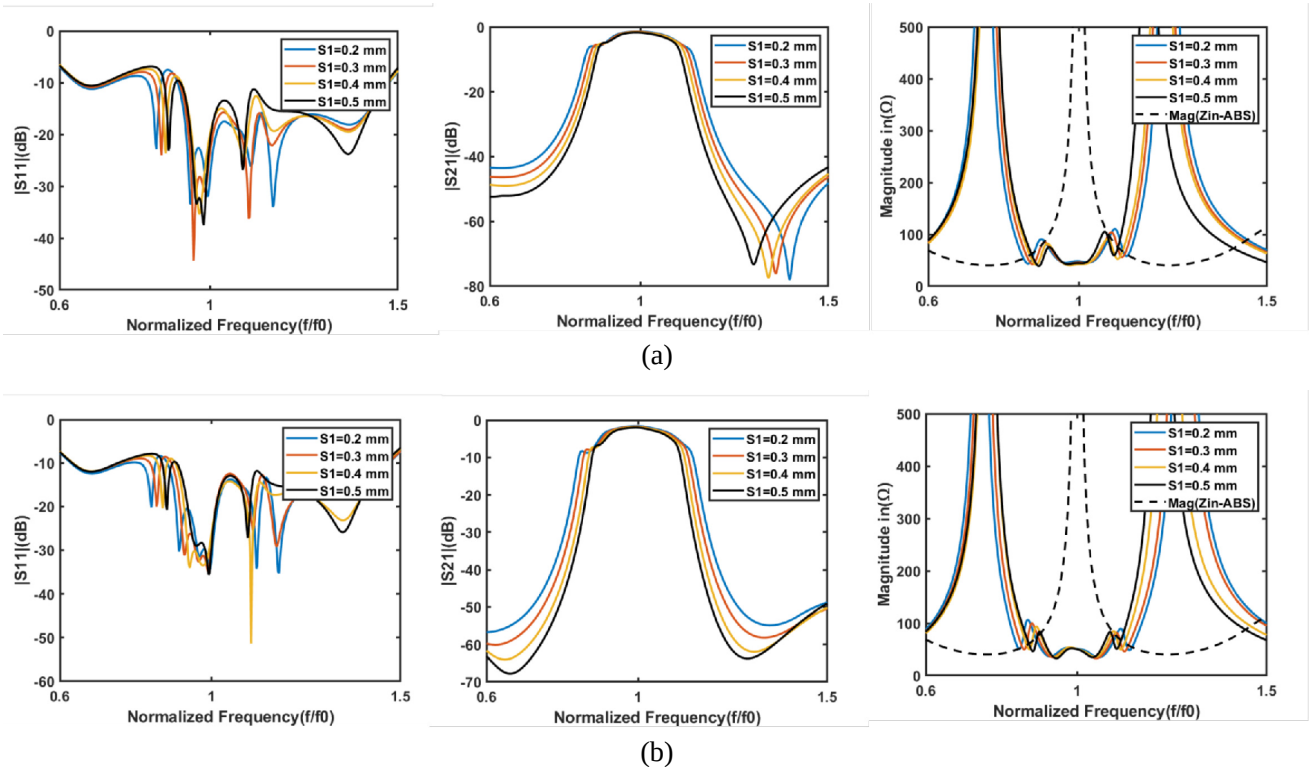

Figure 15. The layout of n-pole U-shaped BPF with the transmission line circuit model of the ABSs connected into the output and input ports, (a) 4th order, (b) 5th order.

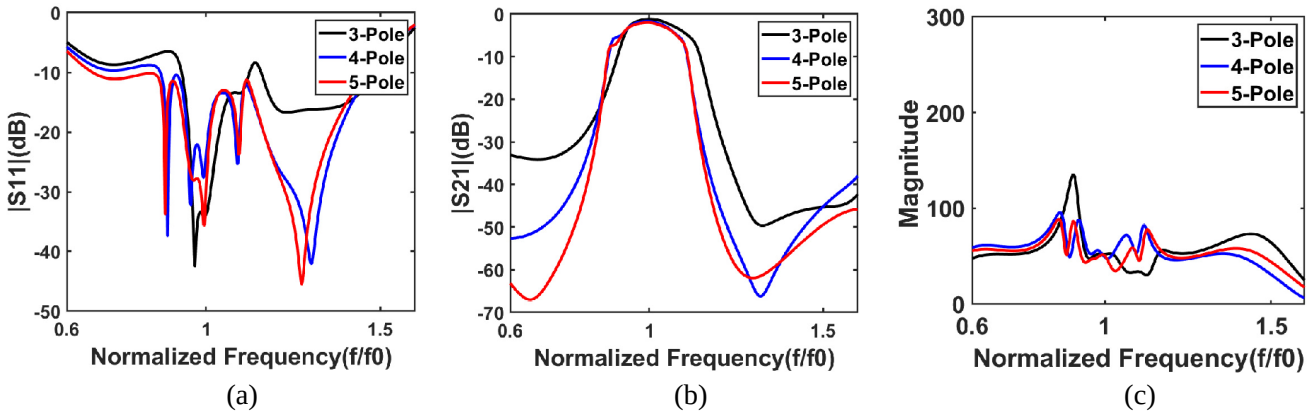

Figure 16. Compares the simulated frequency responses (the reflection and transmission coefficients, and the magnitude of input impedances) of the 3-, 4-, and 5-pole U-shaped quasi-reflectionless filters.

Figure 16 compares the simulated frequency responses (i.e., the transmission and reflection coefficients, and the magnitude of input impedances) of the 3-, 4-, and 5-pole U-shaped quasi-reflectionless filters using the same order ABS. The three simulated filters have almost the same passband bandwidth although the increase in the filter order enhances the far-out-of-band rejection. Accordingly, controlling the passband bandwidth and the absorption ratio requirements can be independently satisfied. Also, fluctuations in the input impedance is lowered with the increase in the filter order.

3.4. Cross-Coupling for Improved Out-of-Band Rejection

The proposed filter response may be further enhanced if the cross-coupling technique is utilized. The cross-coupling method is commonly utilized in the design of microwave filters. To do so, the ABSs are placed close to each other to excite the coupling between them. This method introduces transmission zeros into the filter response because there will be other signal paths between the input and output ports [26], leading to sharper rejection than the same filter without cross-coupling. In [12], source-load coupling is carried out with quasi-reflectionless filters. There are also other ways to implement the cross-coupling as in [3, 7]. Two-path signal cancellation is added to create transmission zeros in the filter response. In this work, transmission zeros are realized by adopting the cross-coupling between the ABSs. Three examples are discussed here. Fig. 17 states where the cross-coupling is introduced. The last stub in each ABS is adjacently vertically placed, converted from Fig. 7(b) to Fig. 17. This method operates to merge these two stubs to a coupled transmission line. Two transmission zeros are added to the response as shown in Fig. 18. One transmission zero is generated at $(f/f_0 = 1.495)$ that means at 5 GHz, while the other transmission zero is not shown here for the sake of simplicity. Interestingly, the cross-coupling also enhances the absorption (i.e., reduce the reflection coefficient). This essentially merges the two stubs into one, as seen in Fig. 18.

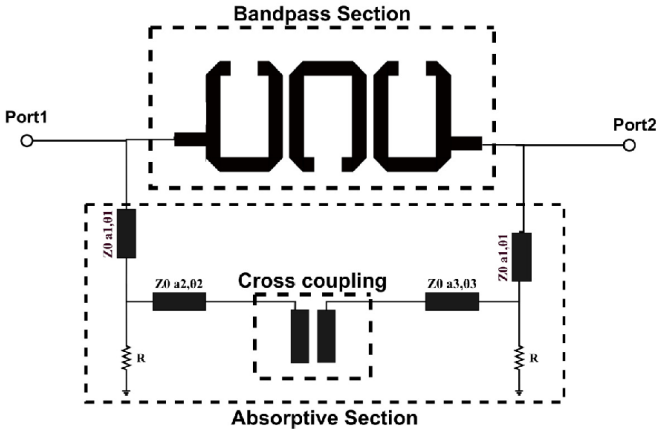

Figure 17. The prototype of 3-pole U-shaped quasi-reflectionless with cross coupling.

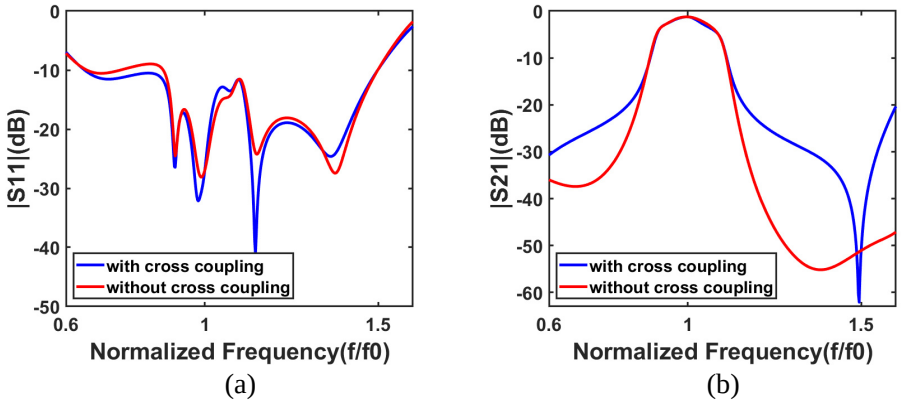

Figure 18. Compares the simulated frequency responses the reflection and transmission coefficients of the 3-pole U-shaped quasi-reflectionless filters with and without cross coupling.

4. DESIGN PROCEDURES

To follow an obvious procedure relying on the analyses discussed above, the steps can be summarized as:

1. Design 3-pole U-shaped BPF with center frequency f_0 and fractional bandwidth FBW.
2. Bandstop filter is synthesized from the lowpass filter prototype [Fig. 3(a)] with f_0 and FBW. Then, the BSF is converted into its ABS counterpart, see Fig. 3 for the conversion process. The ABS consists of three transmission lines with initial impedances (Z_1, Z_2, and Z_3) which are equal to reference impedance Z_0 multiplied by an initial scale parameter ($a1$, $a2$, and $a3$). By default, the scale parameters will be assumed as one. Also, the electrical lengths of the absorptive section are ($\theta 1 = \theta 2 = 90°$, $\theta 3 = 180°$), terminated with absorptive resistor R that can be set to be the same with the termination reference impedance Z_0.
3. Adjust the scale parameters ($a1, a2, a3$) to obtain the magnitude of input impedance as high as possible for the ABS part at BW3 dB of the BPF, see Figs. 8–11. Also, the magnitude of input impedance of the U-shaped quasi-reflectionless BPF is equal to Z_0 at all frequencies which means that matching will occur at in and out of the band, see Figs. 9–12. Eq. (8) can be used to calculate S_{11}.
4. To increase the absorptivity and selectivity of the proposed filter, the technique of cross-coupling can be adopted, see Figs. 17–18. Also, the increase in the order of U-shaped BPF enhances the filter selectivity, see Figs. 15–16.

5. COMPARISON WITH THE STATE-OF-THE-ART

Some works in the literature are reproduced here for the sake of comparison [12, 20], see Fig. 19. The proposed work has less reflection than [12, 20] within the in-band frequency range. The S_{11} is less than 10 dB with the range of normalized frequencies ($f/f_0 = 0.68 - 0.9$), and it is also less than 15 dB in the range of ($f/f_0 = 1.15 - 1.53$).

In [12], S_{11} is about 7 dB at the same normalized range of frequencies. The S_{21} has almost two transmission zeros which enhances the filter selectivity compared to other responses in the same figure,

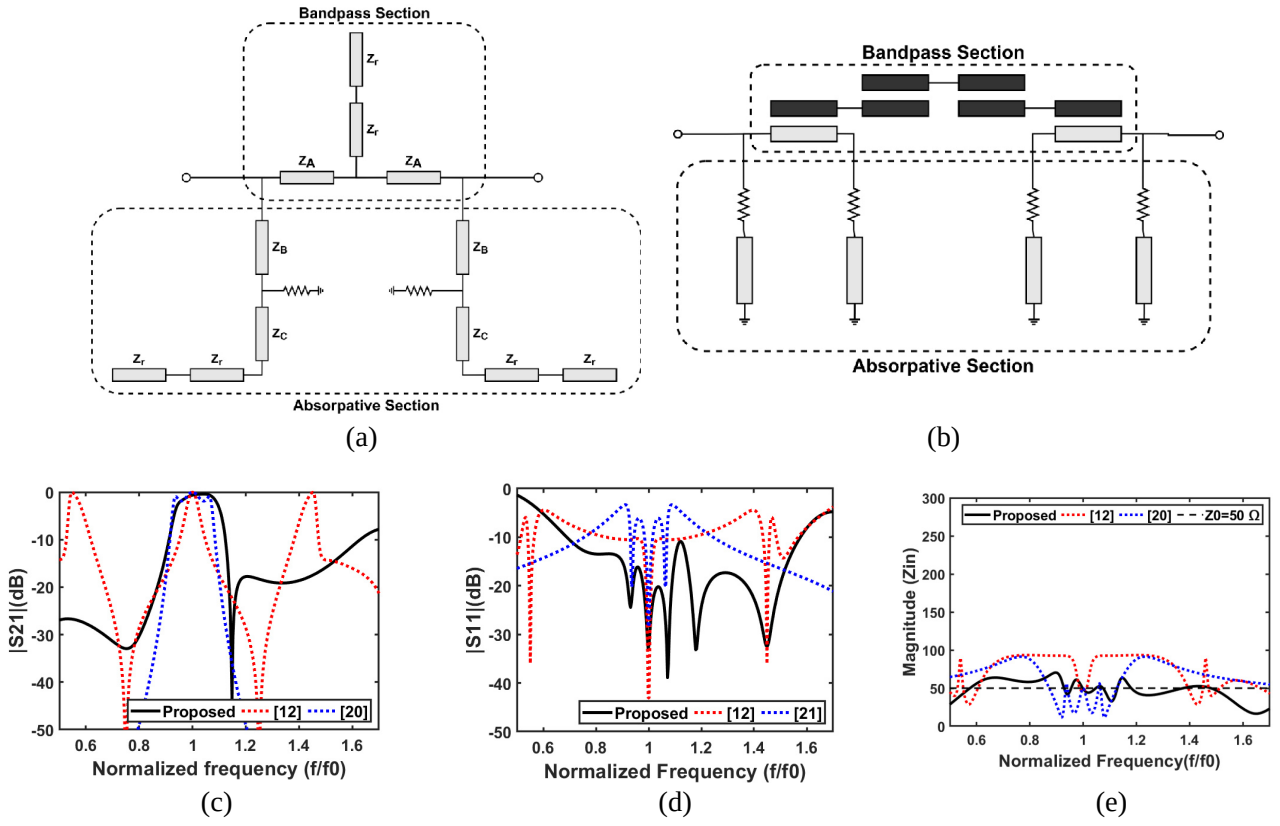

Figure 19. Comparison with previously reported reflectionless filters, (a) schematic of work in [12], (b) schematic of work in [20], (c) $|S_{21}|$ in (dB) response, (d) $|S_{11}|$ in (dB) response, (e) $mag(Z_{in})$ response.

thanks to the cross-coupling. Moreover, Fig. 19(e) shows that the proposed filter has the magnitude of input impedance between 33 Ω and 70 Ω for the range of normalized frequencies (f/f_0 0.5–1.55), whereas in [12] and [20] for the same normalized frequency range, the magnitudes of input impedances are (28 Ω–93.4 Ω) and (11 Ω–91 Ω), respectively. As can be seen, our proposed design offers low variation in the input impedance, resulting in higher transmission S_{21} for in-band and low reflection S_{11} (high absorption) for out-of-band.

6. EXPERIMENTAL VALIDATION

To validate the proposed design, the 3-pole U-shaped quasi-reflectionless bandpass filter is designed, simulated, fabricated, and measured. Fig. 20(a) shows the simulated and fabricated prototypes of the proposed design. An FR4 substrate with relative dielectric constant $\varepsilon_r = 4.6$, dielectric thickness $h = 1.6$ mm, and dielectric loss tangent $\tan(\delta D) = 0.02$ is used. The operating frequency is 3.5 GHz, and the 3 dB fractional bandwidth is 20%. Also, an all-band return loss is better than 10 dB. The Keysight Advanced Design System software (ADS) is utilized to analyze and carry out the schematic and EM designs. Following the design procedure, all physical dimensions of the proposed filter are mentioned in Fig. 20(a).

As expected, the measured results agree very well with the simulated ones. This confirms that the analyses provided above are valid. Figs. 20(a) and (b) compare the measured and simulated results for the transmission and reflection coefficients, respectively. The measured reflection coefficient S_{11} is less than 10 dB from 2.25 GHz to beyond the 5 GHz, not shown here for the sake of simplicity. The discrepancy between the simulated and measured results belongs to many reasons. The proposed work

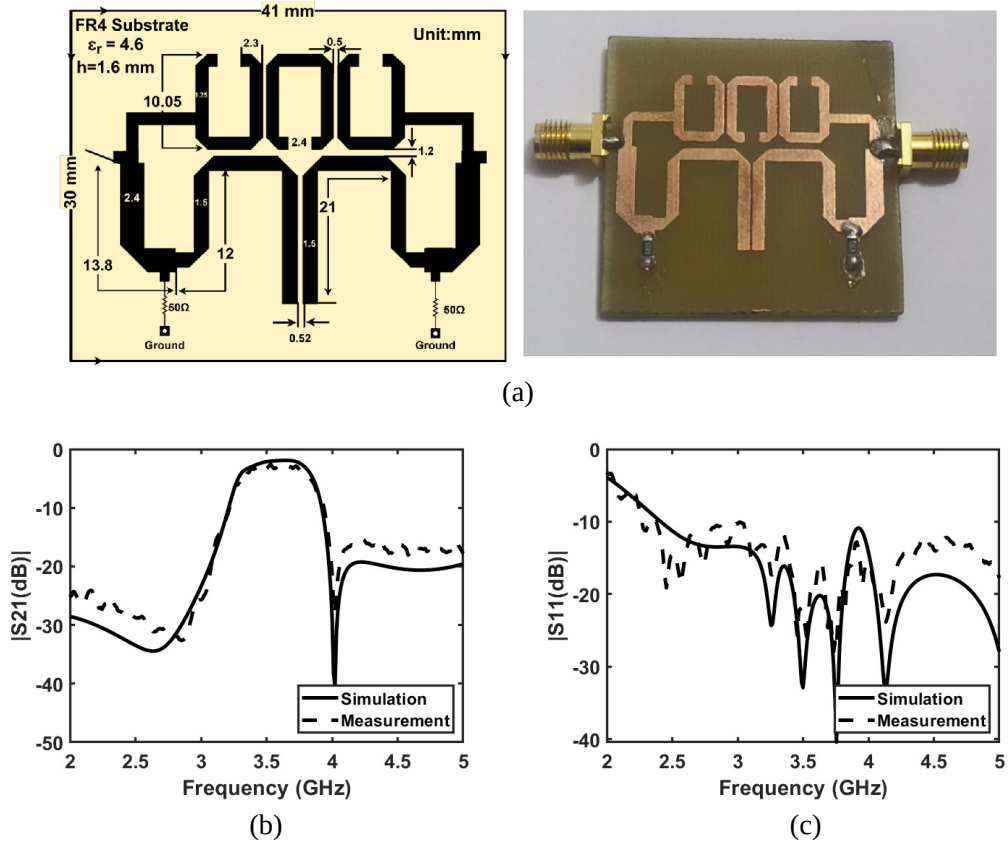

Figure 20. Experimental validations of 3-pole U-shaped quasi-reflectionless BPF. (a) The layout and photograph of the 3-pole quasi-reflectionless BPF. (b) Simulated and measured transmission coefficients S_{21}. (c) Simulated and measured reflection coefficients S_{11}.

was fabricated using the chemical etching process, so there will be some differences in dimensions. Also, the measurements were done with the use of simple VNA, KC901V.

7. CONCLUSION

In this paper, a 3-pole U-shaped quasi-reflectionless filter was proposed, analyzed, designed, fabricated, and tested. Two absorptive stubs (ABSs) were placed at the ports of a conventional U-shaped bandpass filter, based on the complementary duplexer concept. Thus, the response of the proposed work has low reflection coefficient S_{11} at the in-band and out-of-band frequencies, leading to quasi-reflectionless response. First, the filter was studied mathematically especially the absorptive part. Different factors affecting the response were parametrically investigated. Then, the trade-off was made to obtain the optimal design. Afterward, the two absorptive parts were placed close to each other to realize the cross-coupling between the two ports, thereby producing two transmission zeros to enhance the transmission coefficient. An FR4 substrate was used to fabricate the proposed filter. The measured responses were in a good agreement with the simulation ones.

REFERENCES

1. Pozar, D. M., *Microwave Engineering*, 2nd Edition, Wiley, New York, NY, USA, 2012.
2. Morgan, M. A., *Reflectionless Filters*, Artech House, Norwood, MA, USA, 2017.
3. Morgan, M. A. and T. A. Boyd, "Theoretical and experimental study of a new class of reflectionless filter," *IEEE Trans. Microw. Theory Techn.*, Vol. 59, No. 5, 1214–1221, May 2011.
4. Morgan, M. A., W. M. Groves, and T. A. Boyd, "Reflectionless filter topologies supporting arbitrary low-pass ladder prototypes," *IEEE Trans. Circuits Syst. I, Reg. Papers*, Vol. 66, No. 2, 594–604, Feb. 2019.
5. Hong, J.-S., *Advances in Planar Filters Design*, SciTech Publishing, London, U.K., 2019.
6. Lee, J., B. Lee, S. Nam, and J. Lee, "Rigorous design method for symmetric reflectionless filters with arbitrary prescribed transmission response," *IEEE Trans. Microw. Theory Techn.*, Vol. 68, No. 6, 2300–2307, Jun. 2020.
7. Morgan, M. A. and T. A. Boyd, "Reflectionless filter structures," *IEEE Trans. Microw. Theory Techn.*, Vol. 63, No. 4, 1263–1271, Apr. 2015.
8. Luo, C., et al., "Quasi-reflectionless microstrip bandpass filters using bandstop filter for out-of-band improvement," *IEEE Trans. Circuits Syst. II, Exp. Briefs*, Vol. 67, No. 10, 1849–1853, Oct. 2020.
9. Gómez-García, R., J.-M. Muñoz-Ferreras, and D. Psychogiou, "Highorder input-reflectionless bandpass/bandstop filters and multiplexers," *IEEE Trans. Microw. Theory Techn.*, Vol. 67, No. 9, 3683–3695, Sep. 2019.
10. Khalaj-Amirhosseini, M. and M. Taskhiri, "Twofold reflectionless filters of inverse-chebyshev response with arbitrary attenuation," *IEEE Trans. Microw. Theory Techn.*, Vol. 65, No. 11, 4616–4620, Nov. 2017.
11. Gomez-García, R., J. Muno-erreras, and D. Psychogiou, "Split-type input-reflectionless multiband filters," *IEEE Microw. Compon. Lett.*, Vol. 28, No. 11, 981–983, Nov. 2018.
12. Gomez-García, R., J. Munoz-Ferreras, and D. Psychogiou, "Symmetrical quasi-absorptive RF bandpass filters," *IEEE Trans. Microw. Theory Techn.*, Vol. 67, No. 4, 1472–1482, Apr. 2019.
13. Guyette, A. C., I. C. Hunter, R. D. Pollard, and D. R. Jachowski, "Perfectly matched bandstop filters using lossy resonators," *IEEE MTT-S Int. Microw. Symp. Dig.*, 4, Jun. 2005.
14. Shao, J.-Y. and Y.-S. Lin, "Narrowband coupled-line bandstop filter with absorptive stopband," *IEEE Trans. Microw. Theory Techn.*, Vol. 63, No. 10, 3469–3478, Oct. 2015.
15. Lee, T.-H., B. Kim, K. Lee, W. J. Chappell, and J. Lee, "Frequency-tunable low-Q lumped-element resonator bandstop filter with high attenuation," *IEEE Trans. Microw. Theory Techn.*, Vol. 64, No. 11, 3549–3556, Nov. 2016.
16. Hickle, M. D. and D. Peroulis, "Theory and design of frequency-tunable absorptive bandstop filters," *IEEE Trans. Circuits Syst. I, Reg. Papers*, Vol. 65, No. 6, 1862–1874, Jun. 2018.

17. Chien, S.-H. and Y.-S. Lin, "Novel wideband absorptive bandstop filters with good selectivity," *IEEE Access*, Vol. 5, 18847–18861, 2017.
18. Kong, M., Y. Wu, Z. Zhuang, Y. Liu, and A. A. Kishk, "Compact wideband reflective/absorptive bandstop filter with multitransmission zeros," *IEEE Trans. Microw. Theory Techn.*, Vol. 67, No. 2, 482–493, Feb. 2019.
19. Jeong, S., T. Lee, and J. Lee, "Absorptive filter prototype and distributed-element absorptive bandpass filter," *Proc. IEEE MTTS Int. Conf. Numer. Electromagn. Multiphys. Model. Optim. (NEMO)*, 1–4, Aug. 2018.
20. Wu, X., Y. Li, and X. Liu, "High-order dual-port quasi-absorptive microstrip coupled-line bandpass filters," *IEEE Trans. Microw. Theory Techn.*, Vol. 68, No. 4, 1462–1475, Apr. 2020.
21. Wu, X., Y. Li, and X. Liu, "Quasi-reflectionless microstrip bandpass filters with improved passband flatness and out-of-band rejection," *IEEE Access*, Vol. 8, 160500–160514, 2020.
22. Cohn, S. and F. Coale, "Directional channel-separation filters," *Proc. IRE*, Vol. 44, No. 8, 1018–1024, Aug. 1956.
23. Cheng, Y., W. Hong, and K. Wu, "Half mode substrate integrated waveguide (HMSIW) directional filter," *IEEE Microw. Wireless Compon. Lett.*, Vol. 17, No. 7, 504–506, Jul. 2007.
24. Kim, J. P., "Improved design of single-section and cascaded planar directional filters," *IEEE Trans. Microw. Theory Techn.*, Vol. 59, No. 9, 2206–2213, Sep. 2011.
25. Grebennikov, A., *RF and Microwave Transmitter Design*, 231–243, John Wiley and Sons, Inc., 2011.
26. Hong, J.-S. and M. J. Lancaster, *Microstrip Filters for RF/Microwave Applications*, John Wiley & Sons, New York, 2001.